Applied Surface Science 613 (2023) 156000

Contents lists available at ScienceDirect

Applied Surface Science

journal homepage: www.elsevier.com/locate/apsusc

Full Length Article

Analysis of stress in sputter-deposited films using a kinetic model for Cu, Ni, Co, Cr, Mo, W

Tong Su [a,*], Zhaoxia Rao [a], Sarah Berman [a], Diederik Depla [b], Eric Chason [a]

[a] Brown University, School of Engineering, Providence, RI 02912, USA
[b] Department for Solid State Sciences, Ghent University, Krijgslaan 281 (S1), 9000 Ghent, Belgium

ARTICLE INFO

Keywords:
Polycrystalline thin films
Residual stress
Kinetic model
Sputtering deposition

ABSTRACT

Many published studies have quantified film stress evolution for different processing conditions and deposition methods. Here, data from multiple wafer curvature measurements in the literature (for evaporated and sputter-deposited Cu, Ni, Co, Cr, Mo and W) are analyzed in terms of a kinetic model to develop a comprehensive picture of the processes that control film stress. The model includes the effects of film growth kinetics, grain growth and incoming particle energy. Non-linear least squares fitting of the data to this model enables the determination of kinetic parameters that control the stress for each material. The fitting for each material is done in a way that optimizes the parameters simultaneously for all the measurements, both sputtered and evaporated. Parameters that depend only on the material are constrained to have a common value among all the data sets for that material. The validity of the resulting parameters is evaluated by comparing with values estimated from the underlying physical mechanisms.

1. Introduction

Understanding residual stress in thin films is important because of its impact on their performance and reliability. Dependence of the stress on the deposition technique and processing conditions suggests the possibility of controlling the stress. It would be desirable to be able to predict the stress in order to determine the best processing conditions. To this end, we have worked on the development of an analytical model that can be used to analyze and predict the development of film stress.

In previous work, we have described a model for stress in films deposited by non-energetic methods, e.g. evaporation and electrodeposition [1]. This model has recently been used to analyze wafer curvature measurements of stress in multiple materials published in the literature [2]. Non-linear least-squares fitting of the model to the data was used to obtained a set of model parameters that control the stress for each material.

In the current work, we extend the previous work to analyze published measurements of stress in sputter-deposited films (Cu, Ni, Co, Cr, Mo, W). The work uses an extension of the analytical model to include the effects of energetical particles on the stress evolution. Some of the results (Cu, Ni, Cr) are in systems that have also been studied using evaporation. In these cases, we show that the model can describe the stress with a single set of parameters for both types of deposition. This supports the conjecture that the stress-inducing mechanisms due to energetic processes are additive to those described by non-energetic growth processes.

2. Background

Much of the knowledge of thin film stress comes from *in situ* measurements during deposition using wafer curvature techniques. The measured curvature κ is proportional to the stress-thickness, i.e., the product of the thickness-averaged in-plane stress, $\bar{\sigma}$, and the thickness, h_f [3]:

$$\kappa = \frac{6\bar{\sigma}h_f}{M_s h_s^2} \tag{1a}$$

$$\text{where } \bar{\sigma}h_f = \int_0^{h_f} \sigma_{xx}(z, h_f)\, dz \tag{1b}$$

M_s and h_s are the biaxial modulus and thickness of the substrate, respectively and the in-plane stress in each layer at height z is defined as $\sigma_{xx}(z, h_f)$. The stress during growth may change by the addition of new

* Corresponding author.
E-mail address: tong_su@brown.edu (T. Su).

https://doi.org/10.1016/j.apsusc.2022.156000
Received 30 September 2022; Received in revised form 29 November 2022; Accepted 4 December 2022
Available online 10 December 2022

layers in the film (incremental stress) or change in layers that have already been deposited.

There is a large literature of stress measurements [1,4–8] that documents how the stress depends on the processing conditions in different materials for different deposition techniques. For non-energetic deposition, this includes dependence on the growth rate (R), and temperature (T). Low atomic mobility or high deposition rates often produce films with tensile stress while the opposite conditions produce compressive stress. A change in the grain size with thickness can modify the stress in new layers (incremental stress) or in previously-deposited layers. For energetic deposition (sputtering), the energy of the incoming particles also influences the stress which can be controlled by the gas pressure in the chamber, the source to substrate distance, and the discharge voltage. More energetic particles typically lead to more compressive stress [9,10], which is an effective method for mitigating the tensile stress that otherwise develops in deposition of high melting point materials.

Different mechanisms have been proposed to explain the origin of the stress during film growth. Tensile stress has been ascribed to interfacial energy reduction during island coalescence [11] and compressive stress due to the incorporation of excess atoms on the surface into the grain boundary [12]. Chaudhuri [13] has described how grain growth within the layers of the film can create additional tensile stress. Models for sputtering suggest how the subplantation of energetic particles can create compressive stress. For sputtering, the mechanism of "atomic peening" [14] plays an additional role beyond the non-energetic deposition. The momentum transfer from the energetic particles can drive the atoms into the film to form a denser configuration [15] and/or create stress-induced defects. This may occur through processes at the grain boundaries [16–18] or in the bulk of the film itself [10,19,20]. Janssen and Kamminga have suggested that the energetic stress-generating processes can be considered as additive to the processes found in non-energetic growth [21].

3. Stress model

The stress model is based on describing the stress-inducing mechanisms associated with three fundamental processes: 1) the growth of new layers in the film, 2) grain growth in layers that have been deposition and 3) the impact of energetic particles. It has been described elsewhere [1,22,23] so only the final equation is presented here; further details can be found in the supplementary material. The model predicts the slope of the stress-thickness at each thickness of the film, $\frac{d(\bar{\sigma}h_f)}{dh_f}$, due to the additive effect of the different mechanisms:

$$\frac{d(\bar{\sigma}h_f)}{dh_f} = \frac{d(\bar{\sigma}h_f)_{growth}}{dh_f} + \frac{d(\bar{\sigma}h_f)_{gg}}{dh_f} + \frac{d(\bar{\sigma}h_f)_{energetic}}{dh_f} \tag{2}$$

where

$$\frac{d(\bar{\sigma}h_f)_{growth}}{dh_f} = \sigma_C + \left(\sigma_{T,0}\left(\frac{L_{ref}}{L_{surf}(h_f)}\right)^{\frac{1}{2}} - \sigma_C\right) e^{\left(-\frac{\beta D(T)}{RL_{surf}(h_f)}\right)} \tag{2a}$$

$$\frac{d(\bar{\sigma}h_f)_{gg}}{dh_f} = M_f \Delta a \frac{\alpha_1 h_f}{(L_o + \alpha_1 h_f)(L_o + \alpha_2 h_f)} \tag{2b}$$

$$\frac{d(\bar{\sigma}h_f)_{energetic}}{dh_f} = \frac{l}{L_{surf}(h_f)} A_o + \left(1 - \frac{l}{L_{surf}(h_f)}\right) \frac{B_o}{\left(1 + \frac{l}{R\tau_s}\right)} \tag{2c}$$

For comparison with data, the stress-thickness is calculated from numerically integrating this equation.

A brief description of the adjustable parameters in the model is given here. σ_C and $\sigma_{T,0}$ are related to the compressive and tensile stresses generated at the point where new sections of grain boundary are forming between adjacent grains, while βD is a parameter related to the surface kinetics that determines the balance between them. The grain size is assumed to change linearly with the deposited thickness, where $L_o + \alpha_1 h_f$ describes the grain size at the film-substrate interface and $L_o + \alpha_2 h_f$ is the grain size at the film surface (i.e., $L_{surf}(h_f)$). $M_f \Delta a$ is related to the densification associated with subsurface grain growth. A_0 and B_0 are related to energetic particle effects due to densification near the grain boundary and trapping of defects in the bulk of the film, respectively. τ_S is the characteristic time for a defect to diffuse to the surface and annihilate, which depends on the defect diffusivity D_i. R is the growth rate and L_{ref} is a reference grain size (taken as 1 nm). l is the depth at which stress-inducing defects are created.

To illustrate how the different components of the model contribute to the stress, we present some examples of fitting results for sputtered Ni. Fig. 1a shows results for sputtering under conditions of 1.07 Pa, and 0.016 nm/s at room temperature. The average grain size from the fitting is 30 nm. The line labelled 'Total' shows the result obtained from fitting the model to the data. The parameters obtained from the fitting can be found in the supplementary materials. The different components of the fitting model are shown by the different colored lines and described in the legend: they correspond to the contribution of the growth kinetics ($\frac{d(\bar{\sigma}h_f)_{growth}}{dh_f}$ in eq. (2a)), subsurface grain growth ($\frac{d(\bar{\sigma}h_f)_{gg}}{dh_f}$ in eq. (2b)) and energetic processes ($\frac{d(\bar{\sigma}h_f)_{energetic}}{dh_f}$ in eq. (2c)). For the processing conditions in Fig. 1a, the total stress is tensile. According to the different terms in the model, the only tensile stress comes from the grain growth process. The growth kinetics contribute a compressive stress at this growth rate. The contribution of the energetic particles is small, corresponding to the relatively large pressure.

For comparison, the results for sputtering at 0.27 Pa, 0.034 nm/s and room temperature are shown in Fig. 1b. The average grain size from the fitting of this data is 13.2 nm. The components of the stress are represented by the same labels in the legend as described above. Compared to the previous example, the overall stress is compressive for these processing conditions. This is modeled in the fitting by an increase in the energetic particle contribution to the stress because of the lower processing pressure relative to Fig. 1a. Additionally, the contribution of the growth kinetics is slightly more compressive and the contribution of the grain growth is less tensile.

4. Fitting procedure

To determine values for the parameters in the stress model, nonlinear least squares fitting was used to minimize the mean-squared difference between the measured stress-thickness and the model calculations for each material. Multiple sets of data for each material were considered simultaneously by the fitting procedure so that measurements made at different growth rates, temperatures and sputtering pressure were analyzed at the same time to produce a comprehensive set of parameters.

The fitting is done by minimizing the mean-square difference between the model and the data from sets of measurements made for different processing conditions and by different researchers. Each set of data for the stress-thickness at a specific set of processing conditions is identified by the index j and consists of n_j individual data points. The number of sets of data that are being analyzed simultaneously is equal to N_j. The mean squared difference, summed over all the data, is defined as

$$S^2 = \frac{1}{N} \sum_{j=1}^{N_j} \sum_{i=1}^{n_j} \left(y(x_{i,j}) - f(x_{i,j}, \{a\})\right)^2 \tag{3a}$$

$$\text{where } N = \sum_{j=1}^{N_j} \sum_{i=1}^{n_j} 1 \tag{3b}$$

$x_{i,j}$ refers to the independent parameters associated with the i^{th} data point in the j^{th} data set. These include the thickness associated with the

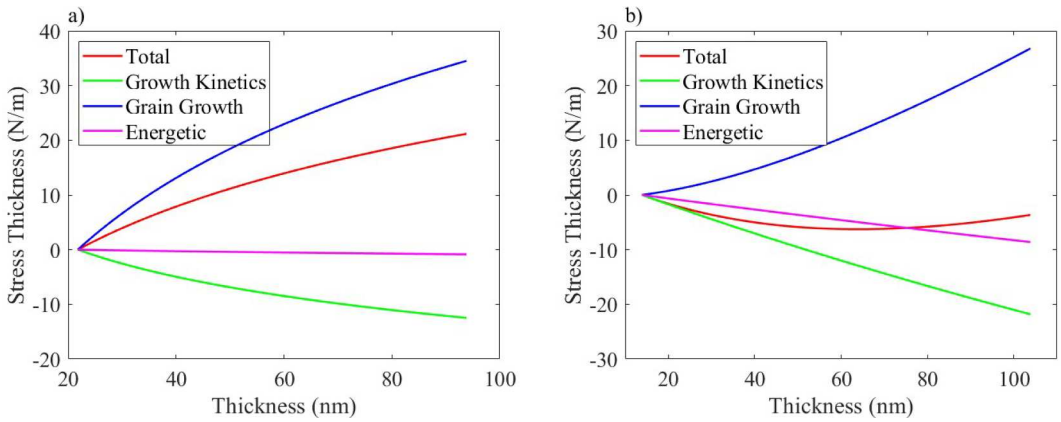

Fig. 1. Plots showing the different components of the stress model, as indicated in the legend, for different processing conditions for sputtered Ni from Lumbeeck [24]. (a) 1.07 Pa 300 K 0.016 nm/s, (b) 0.27 Pa 300 K 0.034 nm/s.

data point as well as the associated processing parameters such as the growth rate, temperature and pressure. $y(x_{i,j})$ refers to the measurement of the stress-thickness for that data point, while $f(x_{i,j}, \{a\})$ refers to the calculation of the stress-thickness from the model with a set of model parameters {a} and the same independent parameters. N is the total number of data points summed over all the data sets. The mean-squared difference is equal to the function χ^2 [25] if each of the differences in eq (3a) is divided by the experimental error associated with that data point. In general, the experimental error was not reported for the curvature measurements. A discussion of the error analysis and its effect on the fitting parameters is contained in Section 6.1.

A set of parameters that minimizes the mean-squared difference is determined by non-linear fitting using the MATLAB® code. For the materials that have data for both evaporated and sputter-deposited films (Cu, Ni and Cr), the combined data are all fit at the same time with the energetic parameters set to zero for the evaporated data. A similar analysis of evaporated films has been described in previous work [2] using the stress model without energetic parameters. The fitting results for the different materials are described in Section 5 and the supplementary material. The significance of these parameters and the error associated with them is discussed in Section 6.1.

Some of the model parameters are only material dependent and are not influenced by the processing conditions. These parameters were made to have a single value when fitting all the data for the same material. This include the parameters $\sigma_{T,0}$, βD and $M_f\Delta a$ for non-energetic growth and D_i for energetic deposition. The other parameters (σ_C, L_0, α_1 and α_2) are processing-dependent parameters and are allowed to have different values for each set of processing conditions.

The energetic parameters A_0, B_0 and l are defined by the scattering of the energetic species with the sputtering gas. Hence, they depend on the pressure and the target-to-substrate distance. Strictly speaking they will also depend on the discharge voltage but the effect on the discharge voltage is rather small. In order to reduce the number of fitting parameters, for each material we assume that the parameters vary linearly with the pressure above a threshold value defined as P_0. Therefore, for a given pressure p the value of A_0 is A^* $(1 - p/P_0)$ where A^* is the fitting parameter that has only one value for each material. Similar treatments are performed for the other energetic parameters so that $B_0 = B^*$ $(1 - p/P_0)$ and $l = l^*$ $(1 - p/P_0)$. The energy also depends linearly on the target-substrate distance, but most studies are done by varying the sputtering pressure. For the studies of multiple growth conditions performed by the same research group, the distance is the same for all the measurements. For all the studies analyzed in this work, the reported target-substrate distances are in a relatively narrow range of 16–18 cm, so that only the variation in the pressure was considered in the modeling.

For measurements made at different temperatures, βD is assumed to have a temperature dependence given by

$$\beta D(T) = \frac{(\beta D)_0}{kT} \exp\left(-\frac{E_A}{kT}\right) \tag{4}$$

Therefore, two fitting parameters ($(\beta D)_0$ and E_A) are obtained from fitting data taken at multiple temperatures. Sets of measurements made at one deposition temperature only need one parameter for βD. In Section 5, the data sets for Cu, Ni and Cr have measurements made at multiple temperatures while Co, Mo and W were all measured at room temperature.

The stress-thickness evolution is calculated by numerically integrating the expression for the derivative in eq. (2). This requires specification of a constant of integration which is a fitting parameter. Since the growth kinetic stress-generating mechanisms in the model assume that the film is continuous and uniform, the fitting is done over the range of thickness after coalescence has occurred, i.e., after the initial tensile peak in the data. The range of thickness that is covered by the fitting is shown by the solid lines on the figures in Section 5.

Least-squares fitting requires initial guesses for the parameters which are estimated from the physical properties of the material, the experimental data and experience with other systems. The fitting procedure allows the parameters to vary freely to obtain the values that give the best agreement with the measurements. With a few exceptions, the fitting is not biased to align with our expectations of how the parameters should depend on processing conditions. Rather, we allow it to be unconstrained and then look at the resulting parameters for different materials to see how their behavior correlates with underlying physical mechanisms. Note that this is not the case for two of the parameters: $M_f\Delta a$ is only allowed to vary by ±20 % from estimates based on the biaxial modulus and the parameter controlling the implantation depth, l_0, is allowed to vary no more than 150 % from values estimated using SIMTRA [26] and SRIM [27].

5. Results of fitting

The results of fitting the model to multiple sets of data in the literature are shown in Fig. 2(a)–(f) for Cu, Ni, Co, Cr, Mo and W, respectively. The symbols represent the data and the solid lines represent the results of fitting to the model. Some of the data sets (Co [28], Mo [29] and W [30]) only consist of results for sputter-deposited films while others (Cu [31–37], Ni [24,38,39] and Cr [11,40,41]) include results for both evaporated and sputter-deposited materials.

Tables with the fitting parameters and the associated error bars for each metal are presented in the supplementary material. These tables also indicate the source of each data set, corresponding to the colors in the figure, and the associated deposition conditions.

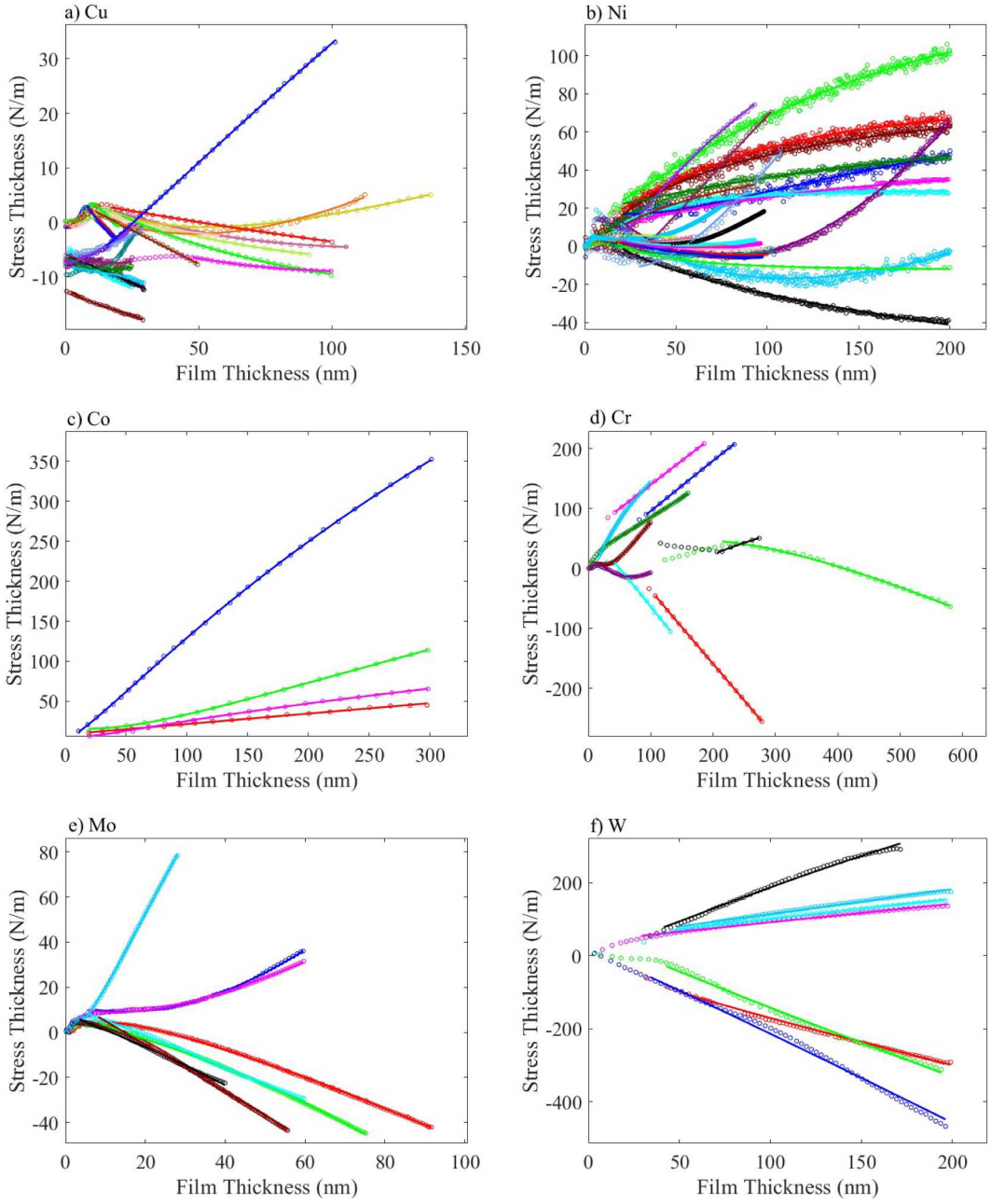

Fig. 2. Data (symbols) and model fit (line) for (a) Cu, (b) Ni, (c) Co, (d) Cr, (e) Mo and (f) W. The processing conditions and source of the data corresponding to each color in the figure can be found in the corresponding tables in the supplemental material.

6. Discussion of results

The agreement between the fitting results and the data in Section 5 shows that the stress model is able to account for a wide range of processing conditions, material parameters and microstructural evolution within a single framework. The fact that some parameters can be kept common for multiple experiments, even those done by different groups, suggests that these are truly material-dependent properties. Furthermore, the model is able to simultaneously fit data from both evaporation and sputter-deposition with a single set of common parameters where the data is available (Cu, Ni and Cr). This supports the assumption that the stress-inducing effects of energetic particles (sputtering) can be considered as additive to those of non-energetic growth or grain growth, consistent with the suggestion of Janssen and Kamminga [21]. Fitting the energetic and non-energetic data separately did not improve the overall quality of the fit.

The fitting parameters were mostly allowed to vary freely and were not constrained to have prescribed values (with the few exceptions discussed in Section 4). In the following sections, we discuss the significance of the parameters resulting from the fitting process and what can be learned from the trends in the parameters for different materials.

6.1. *Significance of fitting parameters*

To start this discussion, we first consider the significance of the parameters obtained from fitting. The fitting procedure produces a set of parameters that minimizes the mean-squared difference between the model and the data, but there may be other sets that produce fits that are also good. The sensitivity of the mean-squared difference to changing the parameters has been discussed previously for the fitting of films deposited by non-energetic evaporation [2]. The analysis there shows that if one parameter is changed by a fixed amount, the other parameters

can readjust to reduce the effect on the mean-squared difference. This means that the minimum is broad in parameter space and many sets of parameters can give similarly low values for the mean-squared difference. The parameters presented in this work should therefore be thought of as a set of reasonable values but not ones that absolutely minimize the mean-squared difference.

For systems in which the deviation between the model and the data is only due to random experimental error, the quality of the fit can be estimated from the value of χ^2. An estimate of the random experimental error can be obtained from the data by taking the variance of the difference between the measurements and a straight line in a region where the slope of the stress-thickness is relatively constant. Using this approach, we estimated the random experimental error of the stress-thickness measurements to vary over a relatively wide range of 0.1–20 J/m. However, the assumption of random errors is not appropriate for this work since it ignores other sources of error. In the first place, the model is not perfect and we expect that there are systematic deviations between the experiments and the model (e.g., the assumption of linear grain growth kinetics). In addition, when analyzing measurements made by different groups there may be errors in the accuracy or calibration of the stress measuring apparatus. This will lead to another systematic source of error when the individual data sets are united into a single comprehensive data set. For this reason, we cannot directly determine the confidence in the fit based on the χ^2 value.

Similarly, the standard deviation associated with each parameter can also be estimated using propagation of errors if the deviation is due to random experimental error [25]. This is done by analyzing how the χ^2 values change when the parameters are displaced from their minimum values. The associated curvature matrix is defined as

$$\alpha_{i,j} = \frac{1}{2}\frac{\partial^2\chi^2}{\partial a_j \partial a_i} \tag{5}$$

where a_j and a_i refer to parameters in the model and the error matrix ($\varepsilon_{i,j}$) is defined as the inverse of $\alpha_{i,j}$. The error on the j^{th} parameter Δa_j is given by [25]

$$\Delta a_j^2 = \sum_{i=1}^{n}\left(\sum_{l=1}^{m}\frac{1}{\Delta_i}\varepsilon_{j,l}\frac{\partial}{\partial a_l}f(x_i,\{a\})\right)^2 \tag{6}$$

where the sums are over all the data points (indexed by i) and parameters (indexed by l). Δ_i is the experimental error for each of the data points. As discussed above, the deviation between the model and data is not due only to random error so we can not exactly calculate the parameter error using eq. (6). Nevertheless, we can use this approach to calculate the curvature of the χ^2 matrix and estimate the relative error for each parameter, even though χ^2 is not correctly normalized and the errors are not random.

To evaluate eq. (6), we need to estimate the experimental error Δ_i. To make this possible, we assume that experiment error is the same for all of the data points for each material (Δ) and therefore $\Delta^2 = \frac{S^2}{\chi^2}$. If we further assume that the χ^2 value is equal to 1 for the best fit parameters, then we can estimate that $\Delta^2 = \frac{S^2}{\chi^2}\widetilde{S^2}$. We do this instead of estimating the experimental error from each data set since we do not believe that random error is the main contribution to the mean-squared difference. The error on each of the parameters (Δa_j) calculated from eq. (6) is proportional to this estimate of the experimental error. The parameter error values obtained from this method are reported with the fitting parameters in the supplemental material.

Because of the large number of model parameters, obtaining a good set of fitting parameters requires a comprehensive set of data that quantifies the stress evolution under a range of processing conditions. For instance, it is not possible to determine the activation energy parameter E_A if there are not measurements made at multiple temperatures. If the geometry of the chambers is different, this can affect the energy of the sputtered species so the pressure dependence of the stress can be affected. However, as discussed above, much of the fitting is done for sets of data that were obtained in the same chamber; data sets taken in other chambers have similar values of the target-sample distance. The fact that common values could be obtained that explained many data sets taken in independent studies suggest that local variations in the processing conditions (e.g., chamber base pressure) do not strongly affect the results.

6.2. Kinetic parameters

To look at the material dependence of the model parameters, we first consider βD, the parameter that depends on the kinetics of non-energetic growth. If we assume that the temperature dependence is given by eq. (4) and that the prefactor $(\beta D)_0$ is similar for all the materials, then ln (βD) at room temperature is proportional to E_A. A plot of ln($\beta D(T = 300$ K)) vs the melting point T_m is shown in Fig. 3a. The data includes analysis of data sets for which we simultaneously fit sputtering and evaporative data (blue circles), only sputtering data (green circles) and only evaporative data (red circles). The value for W is not included in Fig. 3a because the error on this parameter is very large. This is because the low atomic mobility of W means that the compressive stress due to the growth kinetics is insignificant and therefore the kinetic parameter controlling it cannot be determined. Additional discussion of the fitting of the W data is contained in the supplemental material. The plot shows a linear dependence on T_m which is consistent with the observation that the activation energy for diffusion scales with the melting point for many transition metals [42]. This scaling of the activation energy was also observed previously in the analysis of stress in evaporated films [2]. Note that the linear dependence is similar for all the data sets, whether deposited by evaporation or sputtering. This suggests that the kinetic parameter has a similar activation energy for both energetic and non-energetic deposition. A similar trend with the melting point is found in the parameter for the diffusion of defects (D_i), shown in Fig. 3b. This suggests that the activation energy for defect diffusivity is also proportional to the melting temperature, as was found for βD. The shallower slope suggests that the activation energy for defect diffusivity is lower than for βD.

6.3. Grain size evolution

The grain size affects the stress in the model both at the surface and through the evolution of the grain size in the bulk of the film. Importantly, if the grain size does not change, then the model predicts that the slope of the stress-thickness will not change since the incremental curvature due to growth kinetics (term 1 in eq. (2)) and energetic deposition (terms 3 and 4 in eq. (2)) are otherwise independent of film thickness. Consequently, the model attributes any non-linearity of the stress-thickness vs thickness measurements to either surface or sub-surface grain growth. Because of this, if there are any other sources of non-linearity in the stress-thickness (e.g., surface roughening or void formation), the model may adjust the microstructural evolution to capture this, leading to errors in the results of fitting for the microstructural evolution.

The fitting results for grain growth can be compared with experiments where the data is available. This is the case for Ni [38], Cu [31,32], Co [28] and W [30] where the average grain size in the films was measured using TEM. Fig. 4 shows the results of the measured grain size on the x-axis and the value calculated from the fitting at the same thickness as the measurement on the y-axis. Note that the fitting values for Ni are different than those in the original manuscript [38]. That is because the fitting results here include data from other studies besides the work of Koenig et al. The figure also leaves out the measured grain sizes for Ni at low pressure (0.27 Pa) which had a bimodal grain size distribution. In Cu [32], TEM measurements showed that the average grain size in all the films was similar, ranging from 16.7 to 29.3 nm with an average of 22.5 ± −4 nm. The measured grain size did not vary with

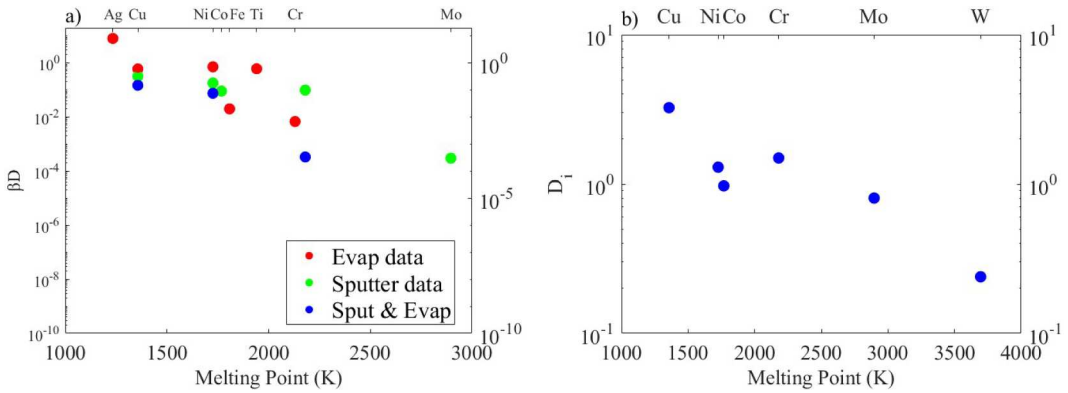

Fig. 3. Fitting parameters for diffusional kinetics determined at room temperature vs melting point of material. (a) βD, (b) D_i.

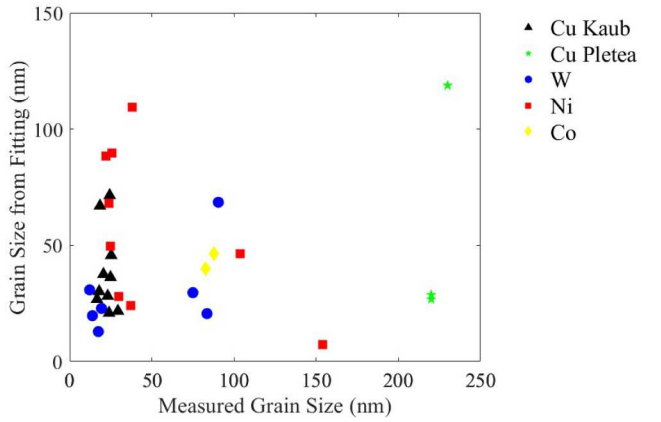

Fig. 4. Grain size from fitting vs measured grain size. The calculation from the fitting parameters is done at the same thickness as the measurement.

the processing conditions because the experiments used a 50 nm Cu buffer layer that was always grown under the same conditions before the growth rate or pressure was changed.

The fitting results in Fig. 4 do not agree exactly with the measured grain size. However, the range of measured values is similar to the fitting values, which shows that the grain sizes produced by the fitting are in a reasonable range. A similar level of agreement between the measured grain size and the fitting was also seen for metal films deposited by evaporation [2].

The grain growth kinetics across multiple studies can be compared to determine if there are any clear trends in the fitting results. One possibility was that higher energy would enhance the nucleation rate of islands, but the fitting does not show a clear dependence on the pressure. In sputtered Cr and Ni, we find that the grain size tends to be smaller for lower pressure (higher particle energy) at the same growth rate. This is also true for sputtered Cu at R = 0.1 nm/s but the opposite behavior is found at R = 0.012 nm/s, i.e., the fitting values predict larger grain size at lower pressures. In Mo, the grain size from fitting is smaller at low pressure for R = 0.06 nm/s but not at the other measured growth rates. The results for Co do not follow either trend. Similarly, we might expect that the grain size would be smaller at higher growth rates (other conditions equal) for each material due to the increased nucleation rate of islands. However, there is not enough data for the sputtered films to determine the dependence on the deposition rate at different pressures. Therefore, although the fitting results appear to give reasonable grain sizes, we cannot reliably identify any trends with the processing conditions. Additional studies that characterize the grain size would be helpful to better understand the connection between the stress and microstructural evolution.

6.4. *Energetic parameters*

To explore the meaning of the parameters for the energetic terms, we show a plot of the A* and B* parameters as a function of the materials' melting point (see Fig. 5). The value of A^* for W is not included because the error on this parameter is very large. As shown in the figure, the parameters become increasingly negative (more compressive) for the materials with a higher melting point with a roughly linear dependence. Note that a similar correlation can be found with the surface binding energy or threshold displacement energy since these also tend to be proportional to the melting temperature [43,44]. This figure therefore suggests that the effect of energetic particles on compressive stress is greater for materials with larger melting points or bond energies. For comparison, we did not find any clear correlation with the atomic mass of the material. Several possibilities for the dependence on melting point are discussed below.

The first effect considered is the energy of the incoming particles. This was estimated by using a combination of SRIM and SIMTRA. We consider two types of particles i.e., sputtered atoms and reflected argon neutrals. The initial energy distribution of the atoms was generated with SRIM. The argon energy was set equal to 400 eV because this energy corresponds with a typical discharge voltage during magnetron sputtering. The default values of the simulation package were used, except for the threshold displacement energy (see Table 1). Subsequently, SIMTRA simulations were performed to calculate the arriving energy and the transfer probability. A generic deposition geometry was chosen with a 10 cm diameter substrate located at a distance of 16 cm from a two-inch planar magnetron. The argon pressure was set at 0.27 Pa. The simulations show that the average energy of the arriving sputtered

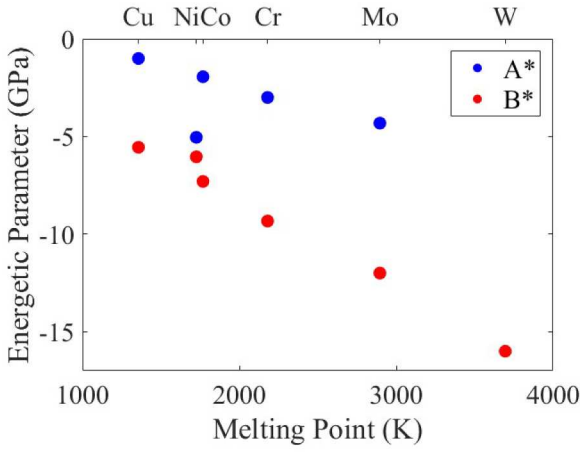

Fig. 5. Fitting parameters A* and B* for energetic terms vs the melting point of the material.

Table 1
Results of the SRIM and SIMTRA simulations. The sputter (Ysput) and backscatter (Yback) yield are shown in column 1 and 2. The transfer probability for the sputtered (T_{sput}) and backscatter atoms (T_{back}) are given in column 3 and 4. The average energy of the sputtered and reflected neutrals are given in column 5 and 6. The displacements per atom (dpa) are shown in the next three columns. The implantation depths of Ar and the sputtered atom are shown in the final two columns. The average displacements per atom ($\overline{dpa}$) is calculated from the dpa for the sputtered atoms (dpa_{sput}) and reflected neutrals (dpa_{back}) using the yields and the transfer probabilities as weighting factors.

	T_m	Y_{sput} at/ion	Y_{back} at/ion	T_{sput}	T_{back}	$\overline{E}_{sput}$ (eV)	$\overline{E}_{back}$ (eV)	dpa_{sput}	dpa_{sput}	$\overline{dpa}$	l_{Ar} nm	L_{atom} nm
Cu	1358	2.21	0.07	0.833	0.77	10.75	16.3	0.399	0.132	0.391	0.4	0.4
Ni	1728	1.63	0.057	0.83	0.763	12.8	12.6	0.338	0.041	0.329	0.4	0.4
Co	1768	1.58	0.049	0.823	0.762	12.31	10.71	0.314	0.03	0.306	0.4	0.4
Cr	2180	1.18	0.038	0.801	0.759	13.2	9.47	0.229	0.014	0.222	0.5	0.4
Mo	2896	0.86	0.132	0.87	0.788	22.64	38.17	0.248	0.099	0.23	0.5	0.6
W	3695	0.76	0.264	0.879	0.811	22.78	89.14	0.117	0.246	0.15	0.5	0.8

atoms increases with increasing melting temperature. The initial energy distribution of sputtered atoms follows a Thompson distribution for which both the average energy and the energy of the mode scales with the surface binding energy, and hence the melting temperature. A similar correlation is not found for the reflected neutrals, although the average energy of neutrals reflected from the two high melting materials i.e., Mo and W, is substantially higher as compared to the other materials. The average energy of the reflected argon neutrals scales linearly with the atomic mass of the target material. This result can be expected based on binary collision physics. The average energy per incoming species can be calculated from the average energy of both species using the appropriate weighting factors. The latter are based on the product of the transfer probability as calculated from SIMTRA and the yield obtained from the SRIM simulations. The average energy increases with the increasing melting temperature which is consistent with the observed trend in Fig. 5.

However, one could argue that the average energy is not a good measure for the defects generated in the materials because only atoms with energy larger than the threshold displacement will be able to generate defects. SRIM simulations were used to correlate dpa (number of displacements per atom) with the energy of the arriving atoms. A linear correlation was found within the energy interval between the threshold displacement energy and the maximum energy of 400 eV. The simulated energy distributions of the arriving species served as weighting distribution to calculate the dpa for each type of arriving species. The average amount of dpa was retrieved in the same way as for the average energy. We find that the average dpa decreases with increasing melting temperature, which is not in agreement with the trend shown in Fig. 5.

To understand why the energetic stress-generation parameters are observed to scale with the average particle energy, but not with the average dpa, we consider how the stress is created. According to the model, the compressive stress is due to the net increase in density in the implanted region, either in the grain boundary or the bulk of the film. There are several ways that this could be occurring. One possibility is that it is due to more of the energetic sputtered atoms or Ar gas being trapped in the higher T_m materials. This is consistent with the value of D_i tending to decrease with larger values of T_m (as shown in Fig. 3b). In addition, the calculated implantation depths (l_{Ar}, l_{atom}) were found to be slightly larger for materials with higher T_m. However, the kinetics of defect trapping are already included in the model, so it isn't clear why the prefactor should scale with melting point. With respect to the role of Ar, measurements of the retained Ar [10,45,46] have not been conclusive in correlating with the resulting film stress.

Alternatively, the dependence of A* and B* on T_m suggests that it might be related to the mobility of the film material. Their increase at higher T_m indicates that there is more compressive stress being generated by the energetic particles in spite of a decreasing average dpa. If there is local relaxation or recombination around the collision cascade, that will reduce the amount of retained damage for materials with higher atomic mobility. Since all the sputtering results were made at room temperature, a higher melting point would correspond to a lower atomic mobility in the material. A reduction in stress relaxation processes for higher melting point temperatures would lead to an increase in stress in the film. In addition, the defects are found to be created at a larger depth for the higher T_m materials which will promote their retention, leading to more compressive stress. These explanations are only conjectures based on the results of the data fitting. In the future, molecular dynamics simulations might be performed to determine the amount of stress induced in films due to energetic particles when relaxation/recombination are also active.

6.5. Other effects on stress evolution

The model that we have applied in this work uses a specific set of mechanisms based on film growth kinetics, grain growth and energetic particle bombardment. However, it should be noted that other effects not considered in the model may contribute to the stress-thickness evolution. For one thing, the model assumes that the film is uniformly thick. However, if there are changes in the morphology of the surface as the film grows, this could modify the stress in the film. The effect of surface roughness on stress evolution has not been systematically studied to our knowledge.

In addition, the temperature of films deposited by sputter deposition may rise during growth. In the measurements that are analyzed here, the degree of heating is not reported so its effect cannot be determined exactly. To estimate its magnitude, we considered the reported change in stress-thickness when sputtering was stopped for Ta [47] after 400 nm of deposition at 0.12 nm/s and 0.7 Pa. The results suggest that the temperature had increased by 42 °C during sputtering. Measurements of the energy flux during sputtering [48] suggest a temperature increase of 25 – 50 °C for 1000 nm of deposition that increases linearly with the film thickness. Herault et al. [49].

Measured a continuous rise in temperature of 13–22 °C during sputter deposition of Ag at different rates and pressures. Such a continuous temperature rise during deposition would create a small additional compressive stress in the previously-deposited layers which would change the slope of the stress-thickness. This could in turn change the fitting result for the grain growth kinetics. More systematic measurements of the thermal evolution during sputtering are needed before the effect of sample heating could be added to the model.

The model assumes that the compressive stress due to atom diffusion is generated at the top of the grain boundary and that atoms do not diffuse deeper into the film. An alternative version of the model that assumes the case of high atomic mobility has also been developed. Both models were used to fit the same data for stress in evaporated Ni at different growth rates and temperatures [50]. Since both models were able to successfully fit the data, it cannot be determined from the fitting whether the assumption of low or high atomic mobility is better. The low atomic mobility assumption was used in the current work because it is consistent with the range of materials and processing conditions studied.

7. Conclusion

A kinetic model that includes the effects of thin film growth kinetics, microstructural evolution and energetic particle impacts has been used to analyze wafer curvature measurements for a number of transition metals. The model is able to explain both sputter-deposited and evaporated films within the same framework, showing that the stress-inducing effects of energetic particles can be considered as additive to other non-energetic effects. The energetic parameters are given a linear dependence on the pressure above a threshold value, reducing the number of fitting parameters.

The parameters that do not depend on the processing conditions are made to have the same value for all the data corresponding to each material. The fact that these parameters can have a single value for multiple studies made by different groups under different conditions, suggests that they are related to fundamental material-dependent processes. This supports the validity of the mechanisms included in the model. The material-dependent parameters related to diffusion kinetics are shown to depend on the materials' melting point, as expected from the underlying physical mechanisms.

Because the deviation between the data and the model is not due to random error, the error on the parameters could not be accurately calculated from the error matrix. Nevertheless, the error determined in this way gives a useful indication of which parameters are more reliably determined by the fitting. Additional experimental studies at a wider range of conditions would be useful to reduce the variation in the fitting parameters.

Ultimately, the fitting program will be implemented as a web-based application that others can use to analyze stress measurements. The determination of the kinetic parameters will enable the stress to be predicted under different processing conditions. A database of results from experiments by the thin film community will provide guidance for growing materials with a controlled stress state.

CRediT authorship contribution statement

Tong Su: Software, Validation, Formal analysis, Investigation, Data curation, Writing – original draft, Writing – review & editing, Visualization. **Zhaoxia Rao:** Software, Validation, Formal analysis. **Sarah Berman:** Software, Investigation. **Diederik Depla:** Writing – review & editing, Methodology. **Eric Chason:** Conceptualization, Methodology, Resources, Writing – original draft, Writing – review & editing, Visualization, Supervision, Project administration, Funding acquisition.

Declaration of Competing Interest

The authors declare that they have no known competing financial interests or personal relationships that could have appeared to influence the work reported in this paper.

Data availability

The data that support the findings of this study are available from the corresponding author upon reasonable request.

Acknowledgements

The effort of EC and ZR was supported by the National Science Foundation (NSF) under Contracts No. DMR-1602491 and DMR-2006422 and TS by DMR-2006422. We thank Prof. Greg Thompson and his group for useful discussions.

Appendix A. Supplementary material

Supplementary data to this article can be found online at https://doi.org/10.1016/j.apsusc.2022.156000.

References

[1] E. Chason, P.R. Guduru, Tutorial: Understanding residual stress in polycrystalline thin films through real-time measurements and physical models, J. Appl. Phys. 119 (2016), 191101.
[2] Z.X. Rao, S. Berman, P.L. Yang, D. Depla, E. Chason, Understanding residual stress in thin films: analyzing wafer curvature measurements for Ag, Cu, Ni, Fe, Ti, and Cr with a kinetic model, J. Appl. Phys. 130 (2021).
[3] L.B. Freund, S. Suresh, Thin Film Materials: Stress, Defect Formation, and Surface Evolution, Cambridge University Press, Cambridge, England; New York, 2003.
[4] R. Koch, The intrinsic stress of polycrystalline and epitaxial thin metal-films, J. Condens. Matter Phys. 6 (1994) 9519–9550.
[5] A.J. Perry, The state of residual-stress in tin films made by physical vapor-deposition methods - the state-of-the-art, J. Vac. Sci. Technol. 8 (1990) 1351–1358.
[6] M.F. Doerner, W.D. Nix, Stresses and deformation processes in thin-films on substrates, CRC Crit. Rev. Solid State Mater. Sci. 14 (1988) 225–268.
[7] R. Koch, Stress in evaporated and sputtered thin films – a comparison, Surf. Coat. Technol. 204 (2010) 1973–1982.
[8] G. Abadias, E. Chason, J. Keckes, M. Sebastiani, G.B. Thompson, E. Barthel, G. L. Doll, C.E. Murray, C.H. Stoessel, L. Martinu, Review Article: Stress in thin films and coatings: current status, challenges, and prospects, J. Vac. Sci. Technol. 36 (2018), 020801.
[9] Y.G. Shen, Y.W. Mai, D.R. McKenzie, Q.C. Zhang, W.D. McFall, W.E. McBride, Composition, residual stress, and structural properties of thin tungsten nitride films deposited by reactive magnetron sputtering, J. Appl. Phys. 88 (2000) 1380–1388.
[10] J.A. Thornton, D.W. Hoffman, Stress-related effects in thin films, Thin Solid Films 171 (1989) 5–31.
[11] R.W. Hoffman, Stresses in thin-films - relevance of grain-boundaries and impurities, Thin Solid Films 34 (1976) 185–190.
[12] E. Chason, B.W. Sheldon, L.B. Freund, J.A. Floro, S.J. Hearne, Origin of compressive residual stress in polycrystalline thin films, Phys. Rev. Lett. 88 (2002), 156103.
[13] P. Chaudhari, Grain-growth and stress relief in thin-films, J. Vac. Sci. Technol. 9 (1972), 520-&.
[14] F.M. Dheurle, J.M.E. Harper, Note on the origin of intrinsic stresses in films deposited via evaporation and sputtering, Thin Solid Films 171 (1989) 81–92.
[15] K.H. Muller, Stress and microstructure of sputter-deposited thin-films - molecular-dynamics investigations, J. Appl. Phys. 62 (1987) 1796–1799.
[16] G. Knuyt, A model for the behaviour of tensile and compressive residual stresses developed in thin films produced by ion beam-assisted deposition techniques, Thin Solid Films 467 (2004) 275–283.
[17] D. Magnfält, G. Abadias, K. Sarakinos, Atom insertion into grain boundaries and stress generation in physically vapor deposited films, Appl. Phys. Lett. 103 (2013), 051910.
[18] L. Koutsokeras, G. Abadias, Intrinsic stress in ZrN thin films: evaluation of grain boundary contribution from in situ wafer curvature and ex situ x-ray diffraction techniques, J. Appl. Phys. 111 (2012), 093509.
[19] F.M. D'Heurle, Aluminium films deposited by rf sputtering, Metall. Mater. Trans. 1 (1970) 725–732.
[20] H. Windischmann, An intrinsic stress scaling law for polycrystalline thin-films prepared by ion-beam sputtering, J. Appl. Phys. 62 (1987) 1800–1807.
[21] G.C.A.M. Janssen, J.D. Kamminga, Stress in hard metal films, Appl. Phys. Lett. 85 (2004) 3086.
[22] E. Chason, A kinetic analysis of residual stress evolution in polycrystalline thin films, Thin Solid Films 526 (2012) 1–14.
[23] E. Chason, M. Karlson, J.J. Colin, D. Magnfalt, K. Sarakinos, G. Abadias, A kinetic model for stress generation in thin films grown from energetic vapor fluxes, J. Appl. Phys. 119 (2016), 145307.
[24] G. Lumbeeck, A. Delvaux, H. Idrissi, J. Proost, D. Schryvers, Analysis of internal stress build-up during deposition of nanocrystalline Ni thin films using transmission electron microscopy, Thin Solid Films 707 (2020).
[25] K.H. Burrell, Error analysis for parameters determined in nonlinear least-squares fits, Am. J. Phys. 58 (1990) 160–164.
[26] K. Van Aeken, S. Mahieu, D. Depla, The metal flux from a rotating cylindrical magnetron: a Monte Carlo simulation, J. Phys. D 41 (2008).
[27] J.F. Ziegler, M.D. Ziegler, J.P. Biersack, SRIM - The stopping and range of ions in matter (2010), Nucl. Instrum. Methods Phys. Res. B: Beam Interact. Mater. At., 268 (2010) 1818–1823.
[28] M. Pletea, W. Brückner, H. Wendrock, R. Kaltofen, R. Koch, In situ stress evolution of Co films sputtered onto oxidized Si (100) substrates, J. Appl. Phys. 99 (2006), 033509.
[29] A. Fillon, G. Abadias, A. Michel, C. Jaouen, Stress and microstructure evolution during growth of magnetron-sputtered low-mobility metal films: influence of the nucleation conditions, Thin Solid Films 519 (2010) 1655–1661.
[30] J.A. Johnson, T. Su, E. Chason, G.B. Thompson, In situ deposition stress evolution of BCC and beta tungsten thin films, (unpublished).
[31] M. Pletea, W. Brückner, H. Wendrock, R. Kaltofen, Stress evolution during and after sputter deposition of Cu thin films onto Si (100) substrates under various sputtering pressures, J. Appl. Phys. 97 (2005), 054908.
[32] T. Kaub, Z.X. Rao, E. Chason, G.B. Thompson, The influence of deposition parameters on the stress evolution of sputter deposited copper, Surf. Coat. Technol. 357 (2019) 939–946.
[33] A.L. Shull, F. Spaepen, Measurements of stress during vapor deposition of copper and silver thin films and multilayers, J. Appl. Phys. 80 (1996) 6243–6256.

[34] D. Chocyk, T. Zientarski, A. Proszynski, T. Pienkos, L. Gladyszewski, G. Gladyszewski, Evolution of stress and structure in Cu thin films, Cryst. Res. Technol. 40 (2005) 509–516.
[35] S.C. Seel, C.V. Thompson, S.J. Hearne, J.A. Floro, Tensile stress evolution during deposition of Volmer-Weber thin films, J. Appl. Phys. 88 (2000) 7079.
[36] R. Abermann, Measurements of the intrinsic stress in thin metal-films, Vacuum 41 (1990) 1279–1282.
[37] R. Koch, D. Hu, A.K. Das, Compressive stress in polycrystalline Volmer-Weber films, Phys. Rev. Lett. 94 (2005), 146101.
[38] T.R. Koenig, Z.X. Rao, E. Chason, G.J. Tucker, G.B. Thompson, The microstructural and stress evolution in sputter deposited Ni thin films, Surf. Coat. Technol. 412 (2021).
[39] H.Z. Yu, C.V. Thompson, Grain growth and complex stress evolution during Volmer-Weber growth of polycrystalline thin films, Acta Mater. 67 (2014) 189–198.
[40] G. Thurner, R. Abermann, Internal-stress and structure of ultrahigh-vacuum evaporated chromium and iron films and their dependence on substrate-temperature and oxygen partial-pressure during deposition, Thin Solid Films 192 (1990) 277–285.
[41] E. Klokholm, B.S. Berry, Intrinsic stress in evaporated metal films, J. Electrochem. Soc. 115 (1968), 823-&.
[42] R.W. Cahn, P. Haasen, Physical Metallurgy, 4th rev. and enhanced ed., North-Holland, Amsterdam; New York, 1996.
[43] H. Landolt, R. Börnstein, P. Ehrhart, O. Madelung, H. Ullmaier, Numerical Data and Functional Relationships in Science and Technology: New Series, Springer, Berlin; London, 1991.
[44] H.H. Andersen, Depth resolution of sputter profiling, Appl. Phys. 18 (1979) 131–140.
[45] C.C. Fang, F. Jones, V. Prasad, Effect of gas impurity and ion-bombardment on stresses in sputter-deposited thin-films - a molecular-dynamics approach, J. Appl. Phys. 74 (1993) 4472–4482.
[46] P. Catania, R.A. Roy, J.J. Cuomo, Phase-formation and microstructure changes in tantalum thin-films induced by bias sputtering, J. Appl. Phys. 74 (1993) 1008–1014.
[47] A.A. Navid, E. Chason, A.M. Hodge, Evaluation of stress during and after sputter deposition of Cu and Ta films, Surf. Coat. Technol. 205 (2010) 2355–2361.
[48] F. Cougnon, M. Kersemans, W. Van Paepegem, D. Depla, Sputter deposited metal layers embedded in composites-from fundamentals to applications, Coatings 11 (2021).
[49] Q. Herault, I. Gozhyk, M. Balestrieri, H. Montigaud, S. Grachev, R. Lazzari, Kinetics and mechanisms of stress relaxation in sputtered silver thin films, Acta Mater. 221 (2021).
[50] E. Chason, A.M. Engwall, Z. Rao, T. Nishimura, Kinetic model for thin film stress including the effect of grain growth, J. Appl. Phys. 123 (2018).